PAPER • OPEN ACCESS

Experimental demonstration of real-time electron temperature profile control in DIII-D

To cite this article: S. Morosohk *et al* 2025 *Nucl. Fusion* **65** 106031

OPEN ACCESS
IOP Publishing | International Atomic Energy Agency
Nuclear Fusion
Nucl. Fusion 65 (2025) 106031 (14pp)
https://doi.org/10.1088/1741-4326/adf456

Experimental demonstration of real-time electron temperature profile control in DIII-D

S. Morosohk[1,*], **K. Erickson**[2] **and E. Schuster**[3]

[1] Oak Ridge Associated Universities, San Diego, CA, United States of America
[2] Princeton Plasma Physics Laboratory, Princeton, NJ 08540, United States of America
[3] Lehigh University, Bethlehem, PA 18015, United States of America

E-mail: morosohks@fusion.gat.com

Received 12 February 2025, revised 30 June 2025
Accepted for publication 25 July 2025
Published 23 September 2025

Abstract
Future tokamak reactor operation will require the ability to maintain a given plasma scenario for extended periods of time. This will necessitate the capability to react to changes in the plasma state and return the plasma to the target scenario; the principal method to achieve this is through feedback control. Thus, it is necessary to develop and test feedback controllers for the plasma profiles that define a target scenario. In this work, a feedback controller for the electron temperature (T_e) profile is tested experimentally in DIII-D. This experiment relied on the ability to ascertain the electron temperature profile in real time, which was achieved using an observer algorithm. The observer relies on both diagnostic data and a predictive model of the electron temperature profile evolution; this predictive model includes contributions from neural network surrogate models. Because of these dependencies, a number of capabilities needed to be added to the real-time Plasma Control System (PCS) for DIII-D in order to support the T_e profile control experiment. The neural network surrogates needed to be integrated into the PCS to be called in real time. An observer algorithm for the T_e profile needed to be added and connected to the Thomson scattering system to allow access to the current state of the profile in real time. When tested, the observer was shown to produce T_e profiles that are consistent with the shape of the Thomson scattering data while rejecting much of the noise in the diagnostic data. Finally, the controller itself was tested in real time. This experiment showed that the controller is capable of tracking the electron temperature target at locations across the spatial profile.

Keywords: DIII-D, electron temperature profile, LQI control

(Some figures may appear in colour only in the online journal)

* Author to whom any correspondence should be addressed.

1. Introduction

The performance of a plasma scenario depends strongly on the spatial distribution of plasma parameters, not just on their maximum or line-averaged values. Small changes in the shape of the safety factor, density, temperature, or rotation profiles can be the difference between a stable, high-performance plasma and instabilities that can cause a drop in performance or even a disruption. Many scenarios have been developed using feedforward control methods, where the values of the relevant actuators (controllable inputs such as auxiliary heating and current drive systems) are chosen before each shot. This approach can be effective for DIII-D shots where the pulse lengths are only a few seconds. However, as the pulse length increases, so does the likelihood that the profiles deviate from their targets over time; feedforward control has no mechanism for correcting these deviations. As we progress toward reactors that have significantly longer pulses, it will become more and more necessary to develop feedback controllers with the capability to correct for disturbances and maintain profiles for long periods of time [1, 2].

Feedback control uses measurements of the state of the system to adjust the actuator trajectories in real time to drive the system towards a target. Because feedback control has the ability to reject disturbances in the system and return to the target trajectory, it can be run in conjunction with feedforward control and only kick in when the diagnostic readings differ significantly from the target state. A feedback approach has been used to control the electron temperature profile in ASDEX-U using proportional, integral, derivative control [3], in JET using proportional-integral (PI) control [4], and in KSTAR using adaptive control [5]. An optimal controller for the electron temperature (T_e) profile in DIII-D has been developed, and simulation results can be found in [6]. In this work, an experimental demonstration of this controller is presented.

Feedback techniques are useful for their ability to react to experimental disturbances and to return the plasma to its target state; in order to do this, feedback algorithms require that the full state of the system can be determined. However, in practical tokamak applications there are often limitations on how much of the system state can be measured in real time. The electron temperature profile is one quantity that is not trivial to measure in real time. There is currently no sensor available that is capable of directly measuring the spatial variation in the electron temperature without requiring an internal fit; however, the Thomson scattering [7] diagnostic data can provide enough point-wise measurements to reconstruct a profile. This is most commonly done by fitting to a function chosen to match the spatial distribution of the diagnostic data, often a modified hyperbolic tangent [8]. This type of fit can be tuned either manually, or automatically using tools such as those described in [9]. A version of this fitting is available in the DIII-D Plasma Control System (PCS) [10], and could be used by the electron temperature controller. However, a modified hyperbolic tangent fit tends to allow a very close fit of the pedestal region of the T_e profile, but does not have much flexibility to match the shape of the core profile. This is not compatible with the goal of the feedback controller to regulate both the magnitude and shape of the core T_e profile. Thus, a different method of determining the state of the system in real time is necessary.

For this purpose, an observer algorithm was developed to estimate the state of the electron temperature profile. State observers have previously been used to estimate both kinetic [11–13] and magnetic [14, 15] profiles in tokamaks. For this observer of the T_e profile, the extended Kalman filter [16] algorithm was used, and relies on both Thomson scattering data and a predictive model of the T_e profile evolution. The use of both a model and diagnostic data allows the observer to reconstruct a T_e profile that is consistent with the profile shape seen in the Thomson scattering data while also rejecting noise to produce a smooth, physically reasonable result. A demonstration of this observer performing well in simulation can be found in [17].

The performance of this type of observer algorithm is highly dependent on the quality of the predictive model used. This model quality can be improved by the use of machine learning surrogate models, which replicate the calculations of high-fidelity traditional models with inference times fast enough to be useful for real time applications. A variety of machine learning surrogates have been developed in recent years with this type of application in mind [18–20]. In this work, two such surrogates are utilized: NubeamNet [21] is used to determine the effects of neutral beam injection on the plasma (for a description of the neutral beam system on DIII-D, see [22]); and MMMnet [23] is used to calculate the anomalous electron thermal diffusivity. These outputs are then plugged into a transport equation that can be evolved to predict the future state of the electron temperature profile. Details of the integration of the neural network surrogates into the analytical predictive model can be found in [17].

In order to test the performance of the T_e profile controller in experiment in DIII-D, it was necessary to first integrate the T_e profile observer algorithm into the DIII-D PCS to ensure that the state of the T_e profile was available in real time. This also required that both NubeamNet and MMMnet were able to be run in real time and that their predictions were available to the observer. Thus, this paper is organized as follows. In section 2, NubeamNet and MMMnet are integrated into the DIII-D PCS and their calculations are validated in real time. In section 3, the T_e observer algorithm from [17] is added to the PCS and is tested in a piggyback experiment. In section 4, the T_e profile controller algorithm from [6] is tested in a dedicated DIII-D experiment, and the results are presented and analyzed. In section 5, conclusions and future work are discussed.

2. Neural network integration and testing

An algorithm has been added to the DIII-D PCS to run a class of neural networks known as PCAnet with sufficiently fast evaluation time for real-time control applications. The term PCAnet refers to any multi-layer perceptron that has

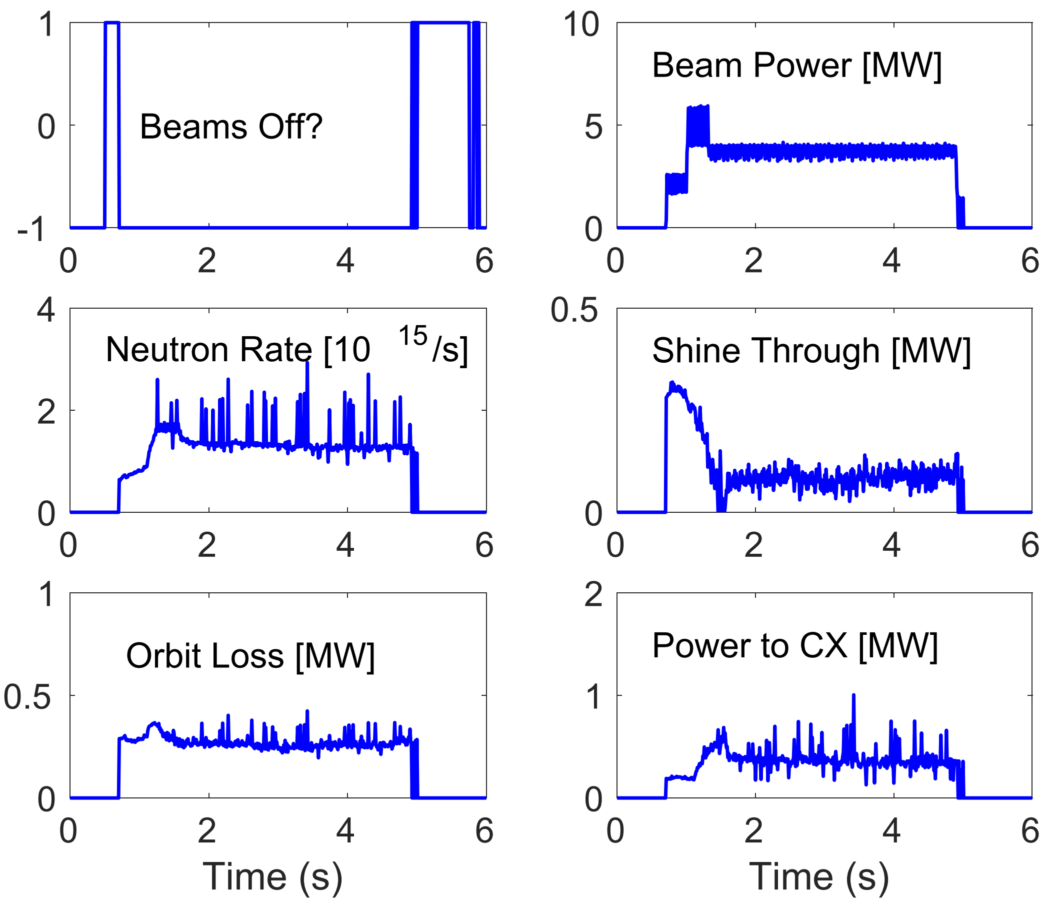

Figure 1. NubeamNet scalar outputs calculated by the DIII-D PCS in real time during shot 195457.

certain qualities (e.g. using a rectified linear unit activation function for the hidden layers) and is saved in a specific file format. In addition, the PCAnet format is able to handle spatially varying data by using a principal component analysis to decompose a profile into a linear combination of scalars. This structure was originally developed for the NSTX version of NubeamNet [18], and has been used for both the DIII-D version of NubeamNet and MMMnet, as well as for other tokamak-related neural network surrogates [24]. The PCAnet PCS algorithm is able to read in from a file how many parallel networks are used, how many layers are in each neural network, how many nodes per layers, all the trained weights connecting the layers, and the coefficients of the principal component analysis for each profile input and output. The current version of the algorithm is able to collect all of the inputs to both NubeamNet and MMMnet, run predictions for both of the networks, save the output data, and send it out for other control algorithms to use in real time. This calculation takes roughly 1 ms combined for both of the NubeamNet and MMMnet; this is sufficiently fast for real-time control of plasma profiles such as the electron temperature and safety factor. In addition, physics operators have the ability to request derivatives of specific outputs of the networks with respect to specific inputs, and the PCS algorithm is able to calculate those derivatives analytically. The algorithm is structured so that any other neural network saved in the PCAnet format can be easily added to the real-time calculation.

The real-time implementation of NubeamNet and MMMnet was tested in experiment. The neural network calculations from the PCS algorithm were tested offline prior to the experiment to make sure they perfectly matched the network calculations in Matlab using the same inputs; the experiment was then carried out to make sure that the algorithm was running well in real time, responding to between-shot changes in settings, and saving the data correctly. The outputs of both networks are shown in figures 1–3 for shot 195457. Figure 1 shows the scalar outputs of NubeamNet as well as the total beam power and error messages that tell the network not to run if, for example, all the neutral beams are turned off. The PCS algorithm is successfully able to run NubeamNet only when at least one of the beams is turned on, and produces reasonable values for all of the scalar outputs. Figure 2 shows the profile outputs of NubeamNet at four different times during the shot, and figure 3 shows the outputs of MMMnet at those same four times; reasonable output values are calculated by both networks for these profile outputs across all four times shown.

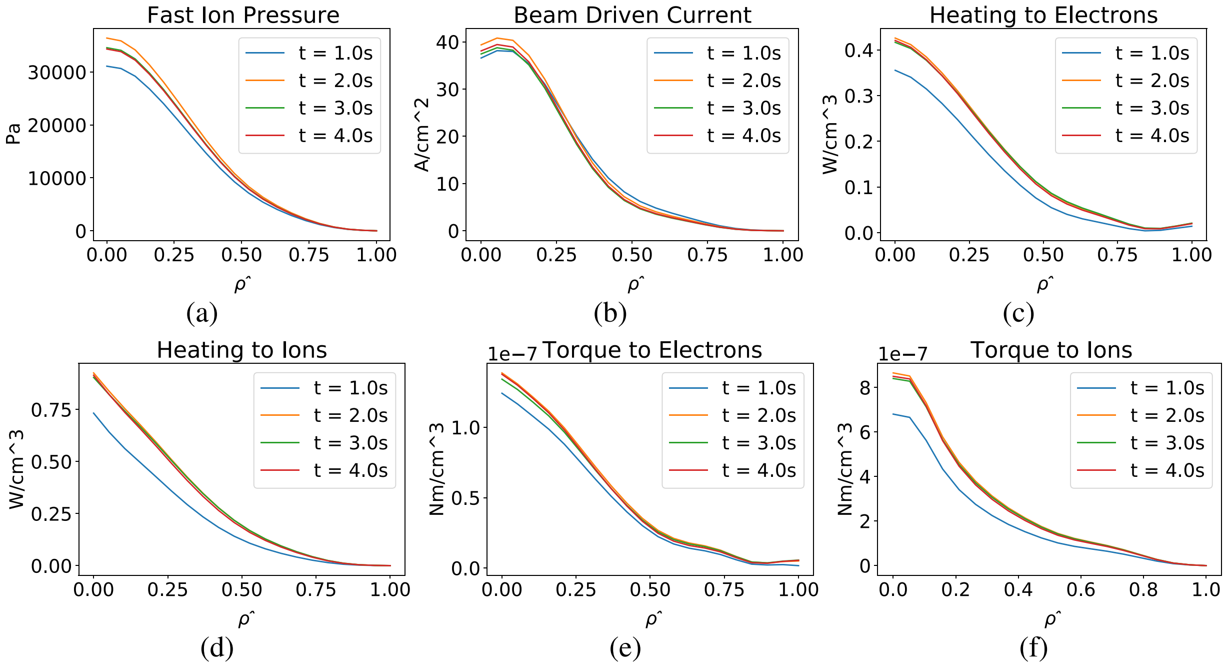

Figure 2. NubeamNet profile outputs calculated by the DIII-D PCS in real time during shot 195457.

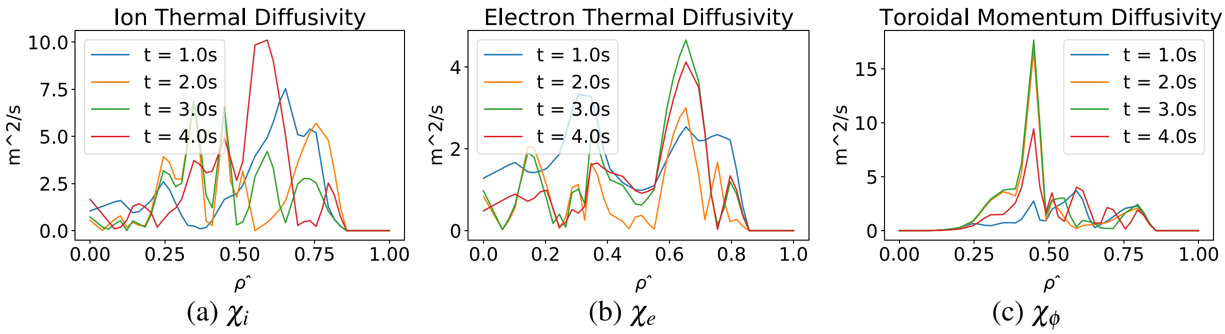

Figure 3. MMMnet outputs calculated by the DIII-D PCS in real time during shot 195457.

3. T_e observer integration and testing

Once the neural networks were validated in real time, the electron temperature observer was then implemented into the PCS. A high level overview of the extended Kalman filter algorithm is shown in figure 4. The prediction of the state vector, comprised of the value of T_e at different spatial locations, is calculated by evolving a transport equation using contributions from traditional models and from NubeamNet and MMMnet. The observer gain is derived using the Jacobian of the predictive model, as well as information about the noise in the system. A correction is then applied to the predicted profile using the Thomson scattering measurements. Only one diagnostic system was used in this initial implementation for simplicity, but data from the ECE system [25] could easily be added in the future for additional robustness in the case where some diagnostic channels are unavailable. For more details on this algorithm see [17]. This implementation was then tested in experiments on DIII-D.

3.1. Shot 195457- Default PCS settings

The internal and measurement noise matrices given to the extended Kalman filter (see equation (28) in [17]) use the following structure,

$$Q = \begin{bmatrix} n & n-1 & n-2 & \dots & 1 \\ n-1 & n-1 & n-2 & \dots & 1 \\ n-2 & n-2 & n-2 & \dots & 1 \\ \vdots & \vdots & \vdots & & \vdots \\ 1 & 1 & 1 & \dots & 1 \end{bmatrix} \times Q_{\mathrm{mag}}, \tag{1}$$

$$R = \begin{bmatrix} n - \frac{y\_rhos(1)}{d\hat{\rho}} & 0 & \dots & 0 \\ 0 & n - \frac{y\_rhos(2)}{d\hat{\rho}} & \dots & 0 \\ \vdots & \vdots & & \vdots \\ 0 & 0 & \dots & 1 \end{bmatrix} \times R_{\mathrm{mag}}, \tag{2}$$

where n is the number of points in the simulation grid evenly spaced from $\hat{\rho} = 0 - 0.9$ and $d\hat{\rho} = \frac{0.9}{n-1}$. The PCS has waveforms to be able to adjust the expected magnitude of noise

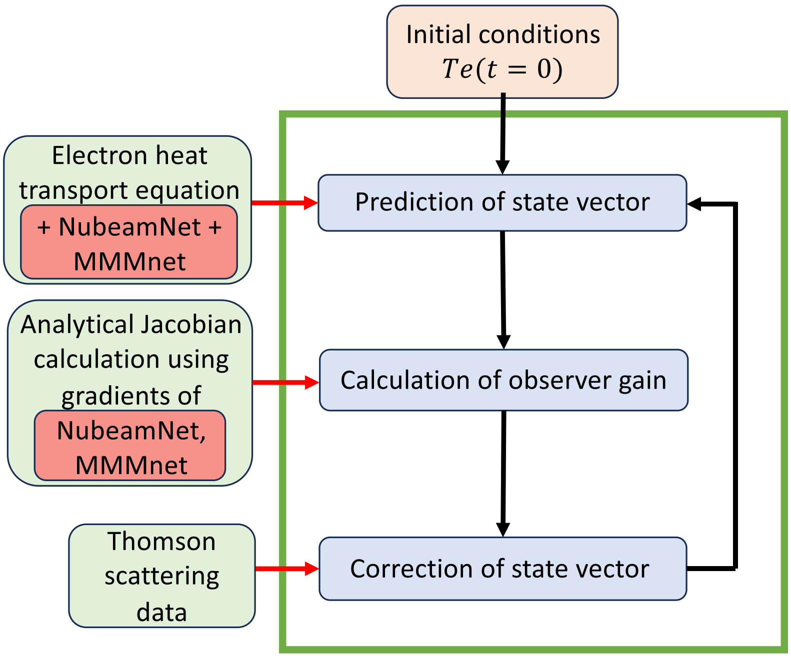

Figure 4. Block diagram showing a high-level workflow of the observer algorithm, including how the predictive model and diagnostic data are integrated.

in the model (Q_{mag}) and diagnostics (R_{mag}), and n before each shot, as well as the number of points n_out that are included in the output y, the spatial locations of the points included in the output y_rhos, and what value of effective charge Z_{eff} will be used by the predictive model to calculate the heat loss due to Bremsstrahlung radiation. The default values in the PCS are $Q_{\text{mag}} = 0.3$, $R_{\text{mag}} = 5$, $n = 10$, $n\_out = 9$, $Z_{\text{eff}} = 1.75$, and $y\_rhos = \begin{bmatrix} 0.1 & 0.2 & 0.3 & 0.4 & 0.5 & 0.6 & 0.7 & 0.8 & 0.9 \end{bmatrix}$. In the offline simulations, one of the goals was to determine the minimum number values that could be included in y_rhos and still achieve observability, or the condition of having enough data to fully constraint the profile reconstruction. Once the observability threshold is known, there is no reason not to use all the measured data available in the real-time implementation; the PCS can run the observer using $n\_out = 10$ in the required calculation time as easily as it can run the observer using the minimum observability requirement of $n\_out = 3$, so y_rhos is extended to include almost every point in the simulation spatial grid. The measured T_e value at $\hat{\rho} = 0$ is excluded because any Thomson scattering channels that do not provide data are seen by the algorithm as measuring $T_e = 0$ at $\hat{\rho} = 0$, which complicated the actual measured T_e value at $\hat{\rho} = 0$. These defaults were chosen because they provided the best match to the Thomson data from shot 192010, which is the shot that was used to test the observer algorithm offline. For other shots with, for example, different shapes, the noise in the model (Q_{mag}) may need to vary to better encapsulate the difference between the equilibrium used by the model and the actual equilibrium of the shot. Note that in simulation, a value of $R_{\text{mag}} = 2$ was found to be sufficient [17], while for experiment we use $R_{\text{mag}} = 5$. The simulations in [17] used post-processed Thomson scattering data, while the experiment uses real-time Thomson scattering data; the post-processing can sometimes introduce significant changes. A higher allowance of noise in the diagnostic data was introduced in the experiment to account for the lack of post-processing. Shot 195457 ran with these default values, and the results are shown in figure 5. For this shot, the observer did a fairly good job of matching the magnitude and shape of the Thomson scattering data using the default PCS settings. This is demonstrated by the high values of r^2, roughly 0.9 or greater where 1 represents a perfect correlation, across all four time points shown.

3.2. *Shot 195465-default PCS settings*

The observer was also tested the next day on a different experiment using the same default values. The results from shot 195465 are shown in figure 6. For this shot, the observer was able to match the magnitude and shape of the Thomson data well at some times in the shot, such as at 1.4 s and 4.4 s. However, the observer noticeably underestimated the magnitude of the Thomson data where $\hat{\rho} < 0.6$ at 3.4 s, and achieved an r^2 value less than 0.8. This was due to the predictive model significantly under-predicting the value of T_e in that range, and the observer only being able to partially make up for it. This can be addressed between shots by adjusting parameters of the predictive model such as Z_{eff}, or parameters of the observer such as Q_{mag} and R_{mag}.

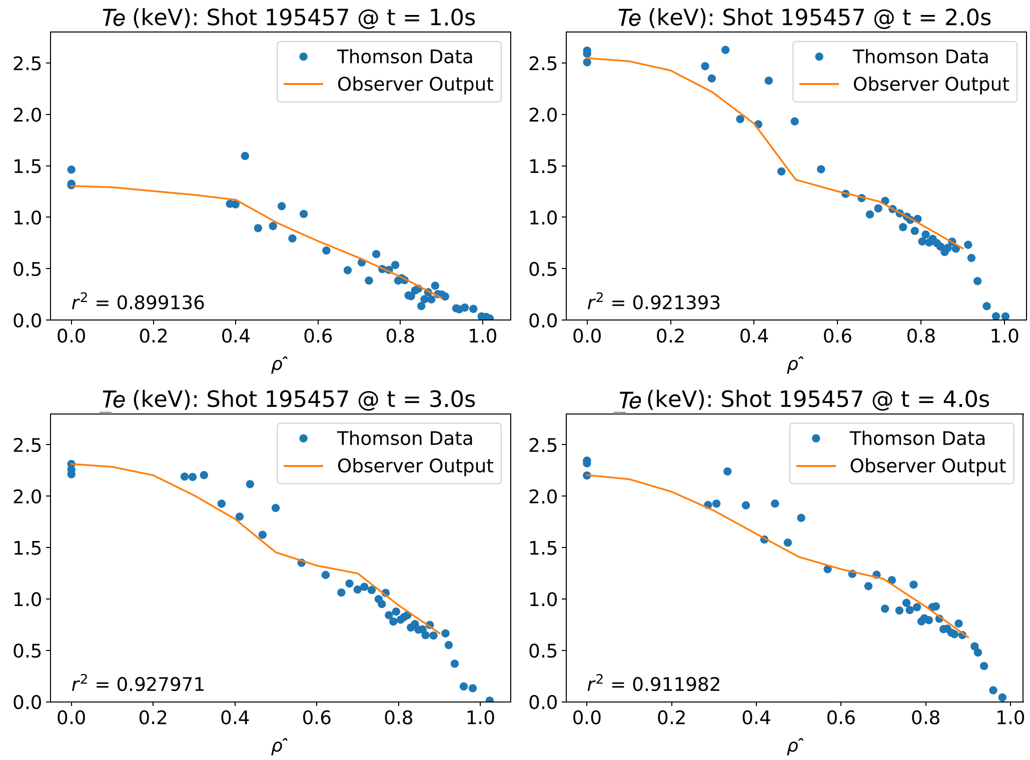

Figure 5. Observer output for shot 195457 using all default PCS values. The coefficient of determination (r^2) metric in the range $0 \leqslant \hat{\rho} \leqslant 0.9$ is used to quantify how well the observer output captures the diagnostic data.

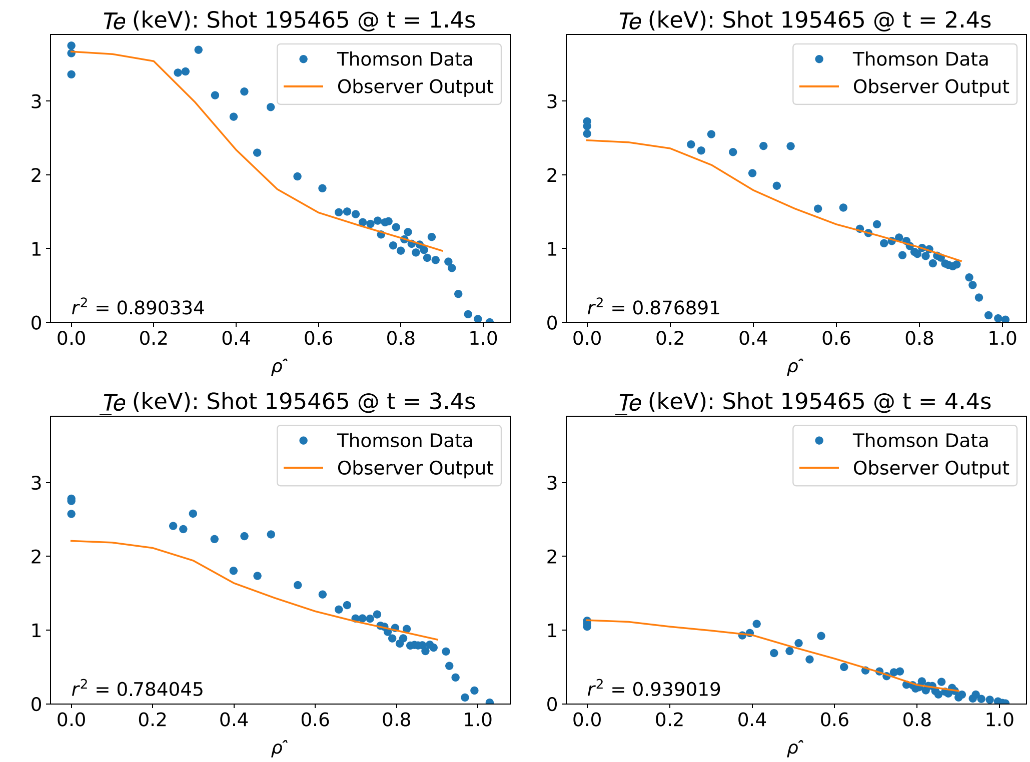

Figure 6. Observer output for shot 195465 using all default PCS values. The coefficient of determination (r^2) metric in the range $0 \leqslant \hat{\rho} \leqslant 0.9$ is used to quantify how well the observer output captures the diagnostic data.

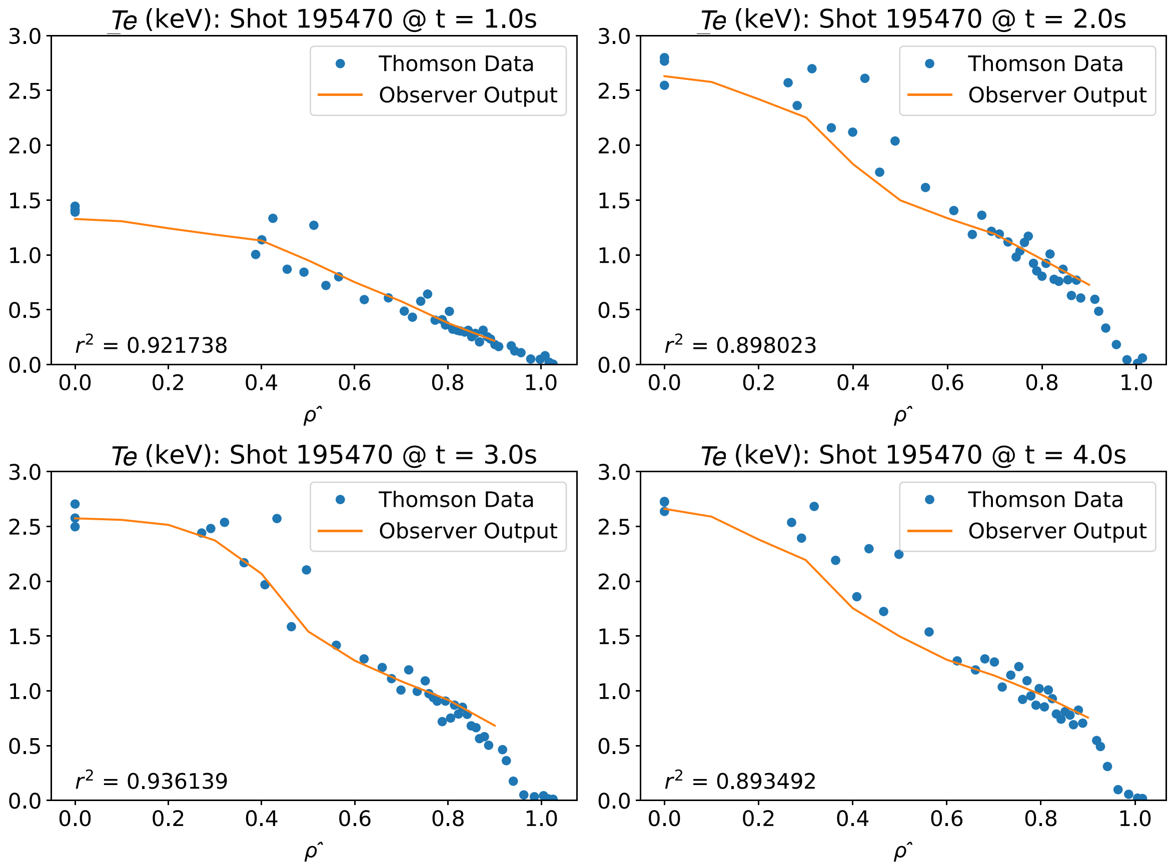

Figure 7. Observer output for shot 195470 using tuned PCS values. The coefficient of determination (r^2) metric in the range $0 \leqslant \hat{\rho} \leqslant 0.9$ is used to quantify how well the observer output captures the diagnostic data.

3.2.1. Shot 195470-tuned PCS settings. After seeing the results from shot 195465, the default PCS settings were adjusted to produce a better match to the Thomson data for this specific experiment. A number of different settings were tried, and the best results were seen on shot 195470. This shot used $Q_{\mathrm{mag}} = 0.5$, $R_{\mathrm{mag}} = 3$, $n = 10$, $n\_out = 9$, $Z_{\mathrm{eff}} = 3.5$, and $y\_rhos = \begin{bmatrix} 0.1 & 0.2 & 0.3 & 0.4 & 0.5 & 0.6 & 0.7 & 0.8 & 0.9 \end{bmatrix}$. The adjusted value of Z_{eff} came from checking the measured value of Z_{eff} from shot 195467, and it was adjusted in the NubeamNet and MMMnet predictions as well as in the observer algorithm. For this shot, the observer was able to match the magnitude and shape of the Thomson data much better ($r^2 > 0.89$ at all times), with significantly less underestimation (see figure 7).

Note that, in this instance, tuning of the PCS settings was performed during the experiment and took several shots to complete. For future experiments that plan to use this capability, this type of tuning can be performed offline in simulation shots prior to the run day to avoid delays caused by the need for tuning this algorithm. Both the observer and the neural network algorithms could be updated in the future to include a real-time calculation of Z_{eff}, eliminating the need to manually tune that parameter.

4. T_e controller testing

An experiment was run on DIII-D to test the T_e profile controller from [6] in real time. This is a linear quadratic integral (LQI) controller that was generated using a linearized model of the coupled magnetic diffusion equation and electron heat transport equation. The linearized model was then used to define the cost function of a minimization problem to synthesize the optimal controller gains. The cost function,

$$J = \int_0^\infty \left[\hat{z}^{\mathrm{T}} Q_{\mathrm{LQI}} \hat{z} + \hat{u}^{\mathrm{T}} R_{\mathrm{LQI}} \hat{u}\right] \mathrm{d}t \tag{3}$$

contains terms to minimize the error between the target and the measured state subject to the weight Q_{LQI} and to minimize the request coming from each actuator subject to the weight R_{LQI}. A more detailed discussion of the controller synthesis can be found in [6]. The workflow of the LQI controller integrated into the PCS is shown in figure 8. The T_e observer discussed in the previous section was used to determine the state of the T_e profile in real time. A reference shot (196108) was run in feedforward as a baseline with $I_p = 1.1$ MA and $B_0 = -2.05$ T.

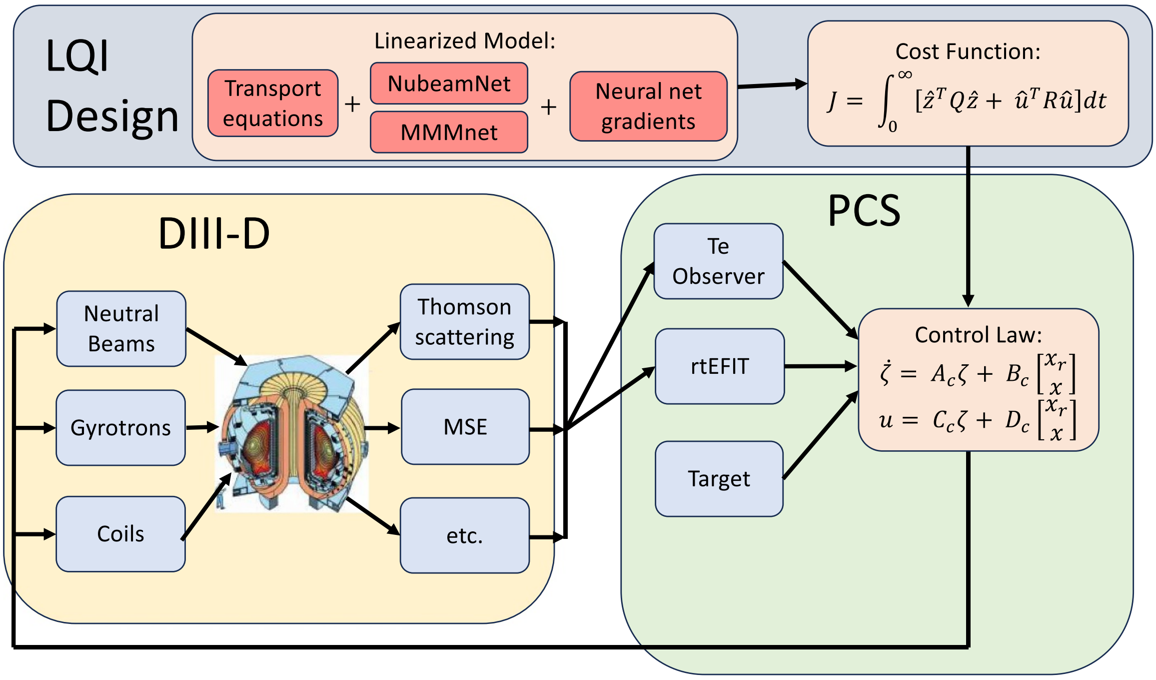

Figure 8. Workflow of designing an LQI controller and testing it in experiment.

All eight beams were available, with the 150 beams aimed off-axis and the 210 beams in the counter-current position. Five gyrotrons were available using X-mode, 2nd harmonic heating deposited between $0.4 \leqslant \hat{\rho} \leqslant 0.5$ for a total of 3 MW coupled heating. Two other shots were run in feedforward: 196115 used more auxiliary power than the baseline and 196118 used less auxiliary power than the baseline. Increasing the auxiliary power led to some MHD stability issues that can lower the temperature, so even though 196115 used more power the core temperature ($\sim\hat{\rho} = 0 - 0.5$) was not actually any higher than the core temperature in 196108. No significant stability issues came up when decreasing the auxiliary power, so the temperature in 196118 is consistently lower across the profile than the temperature in 196108. The observer outputs from 196115 and 196118 were converted to target files that the profile control category of the PCS can read in and attempt to track. Using targets generated from experimental shots that were run the same day ensures that the target T_e profiles are physically reasonable to achieve given the current the machine constraints.

For shot 196119, the same feedforward trajectories as 196108 were programmed up until $t = 2$ s. At two seconds into the shot, feedback was turned on with the target set to the T_e profile values from shot 196118. The T_e values from the feedback shot 196119 (orange) are shown in figure 9 compared to the target 196118 (blue) and the feedforward baseline 196108 (green) at four different spatial locations. In this case, the target T_e values are distinctly lower than the baseline case across all spatial location in the profile after 2 s. After feedback is turned on at 2 s in shot 196119, the controller is very clearly driving the T_e profile to the target across all four spatial locations shown. Some fluctuations are seen in the temperature between 3.5 and 4.5 s, especially at $\hat{\rho} = 0.7$, but every time the temperature deviates from the target the controller is able to adjust the actuators, especially the 330 beams, to correct it.

The actuator values from shot 196119 compared to the target shot 196118 are shown in figures 10 and 11. Note that the powers injected by the 30 L and 30 R beams are exactly the same for shots 196115 and 196116; these beams were not available to control in feedback because of the necessity of getting data from the motional Stark effect diagnostic [26]. The co-current, on-axis beam power requests from the feedback controller were all sent to the 330 beams. The controller was designed to request the largest changes in actuation from the co-current, on-axis neutral beams, because these are the actuators in DIII-D that have the strongest ability to change the value of the electron temperature. This can be seen in figure 11, where most drastic variations in actuator values in response to deviations from the target T_e values are seen in the 330 beams, followed closely by the 210 beams. The 210 beams also have a significant impact on the value of T_e and were thus also weighted highly. Figure 10 shows that the target shot used 1 MW of ECH, but the feedback controller requested almost no ECH, which was weighted lower in the controller design. It replaced that heating power with a combination of co-current and counter-current beam power, and was able to achieve the

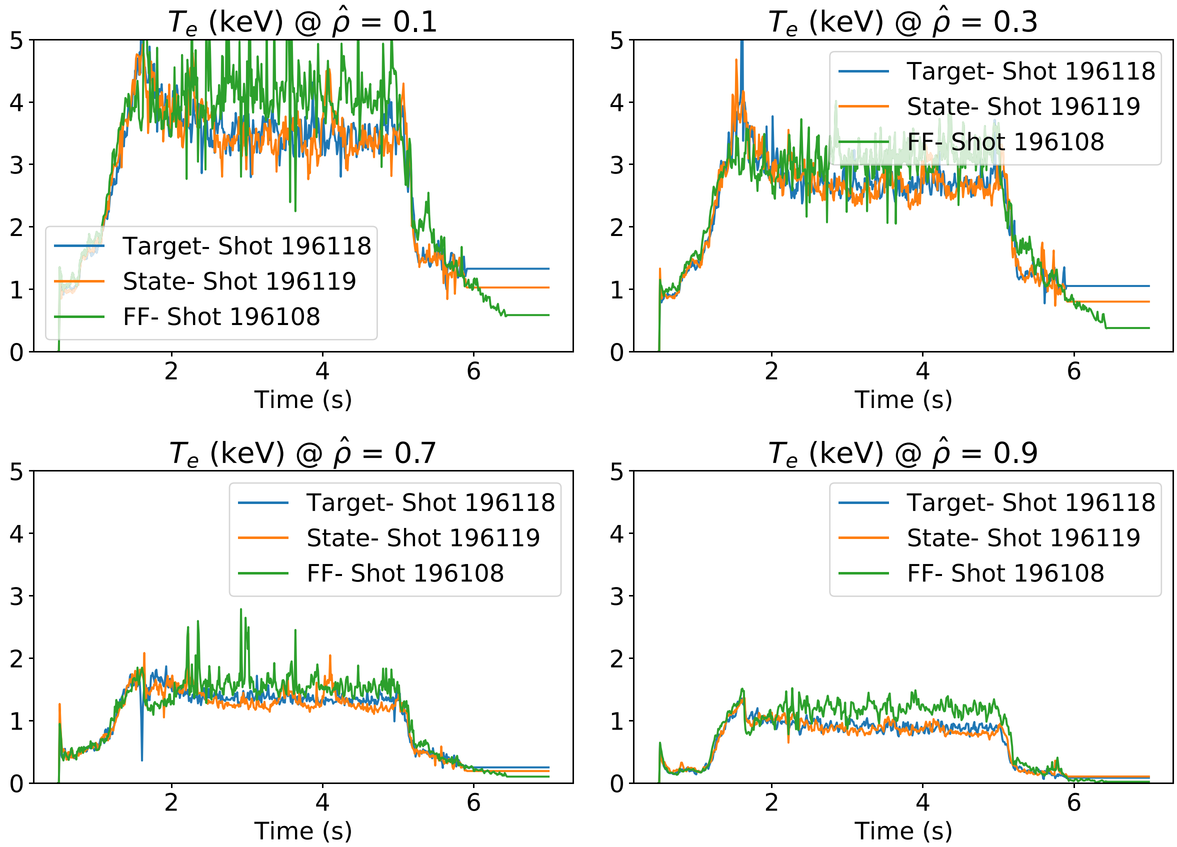

Figure 9. T_e controller results for shot 196119. The controller clearly tracked a target lower than the baseline profile for ∼3 s.

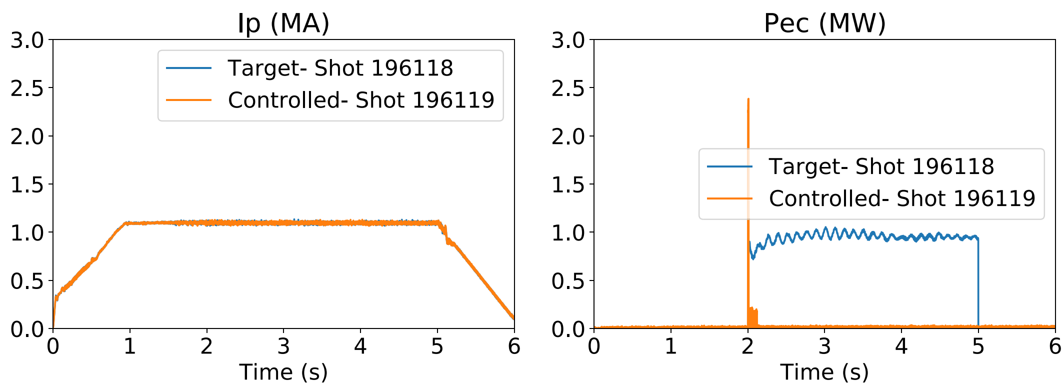

Figure 10. T_e controller current and ECH power for shot 196119. The plasma current for the controlled shot perfectly matched the plasma current for the target shot, while the ECH power for the controlled shot is significantly lower than the target shot.

same T_e profile. This demonstrates that this controller is able to respond as expected in real time to drive the T_e profile to a target and to keep it there.

Another test was run using a target T_e profile that was generated using more auxiliary heating than baseline feedforward T_e profile, although the difference in magnitude between the baseline and the target T_e profiles was not as significant at in the previous case. For shot 196116, the same feedforward trajectories as 196108 were programmed up until $t = 2$ s. At two seconds into the shot, feedback was turned on with the target set to the T_e profile values from shot 196115. The T_e values from the feedback shot 196116 (orange) are shown in figure 12 compared to the target 196115 (blue) and the feedforward baseline 196108 (green) at four different spatial locations. At

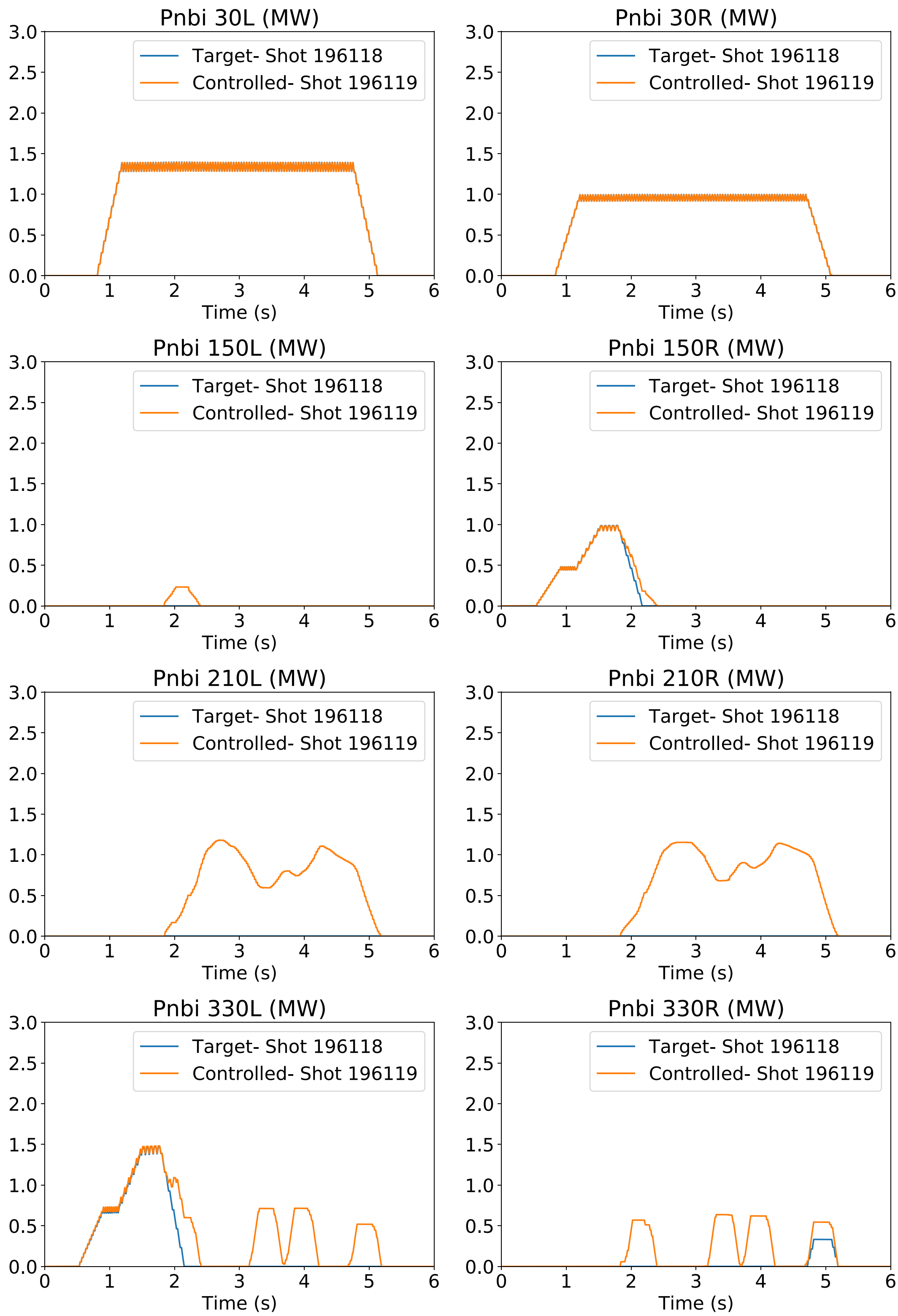

Figure 11. T_e controller neutral beam powers for shot 196119. The 30 L and 30 R beams are not included in feedback, so the controlled case perfectly matches the target case. After 2 s, there is a significant power request from the 210 and 330 beams in the controlled case where no power was injected in the target case.

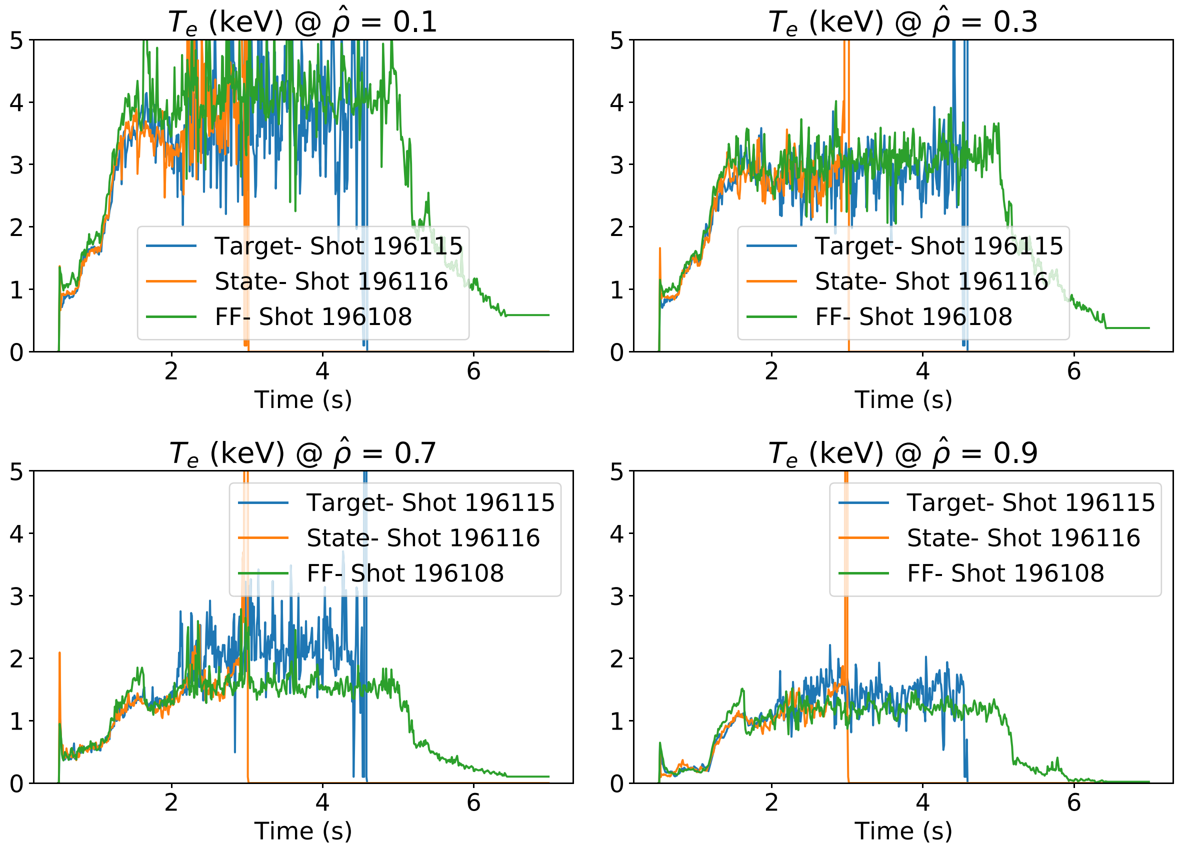

Figure 12. T_e controller results for shot 196116. The controller failed at 3 s due to a lack of data from the T_e observer just before 3 s. This loss of data was caused by a PCS issue. However, in the time from 2–3 s, T_e appears to me moving towards the target values, especially at $\hat{\rho} = 0.7$ and $\hat{\rho} = 0.9$.

$\hat{\rho} = 0.1$ and $\hat{\rho} = 0.3$ the T_e values of the target shot appear to be slightly lower than the baseline; however, with the noise coming from the observer output there is not enough of a difference between the target and the baseline to tell if the controller is having a significant effect. Closer to the edge of the profile, at $\hat{\rho} = 0.7$ and $\hat{\rho} = 0.9$, the target is very clearly higher than the baseline, and between 2 and 3 s the controller appears to be increasing the value of T_e and driving it towards the target. The actuator values from shot 196116 compared to the target shot 196115 are shown in figures 13 and 14.

Unfortunately, the observer failed right before 3 s so the controller did not have enough information to function correctly for the rest of the shot; it was effectively trying to match a T_e value of zero. This failure seems to have stemmed from a numerical instability caused by the explicit characteristics of the heat transport equation solver. Possible fixes for this numerical issue include speeding up the real time calculation so that the observer algorithm can run on a smaller time step, or using a fully implicit heat transport equation solver in the observer. Neither of these fixes are trivial, and were therefore not able to be implemented before the completion of the experiment. While not a full fix, the profile control algorithm could be updated in the future to recognize when it is receiving bad data and stop active control.

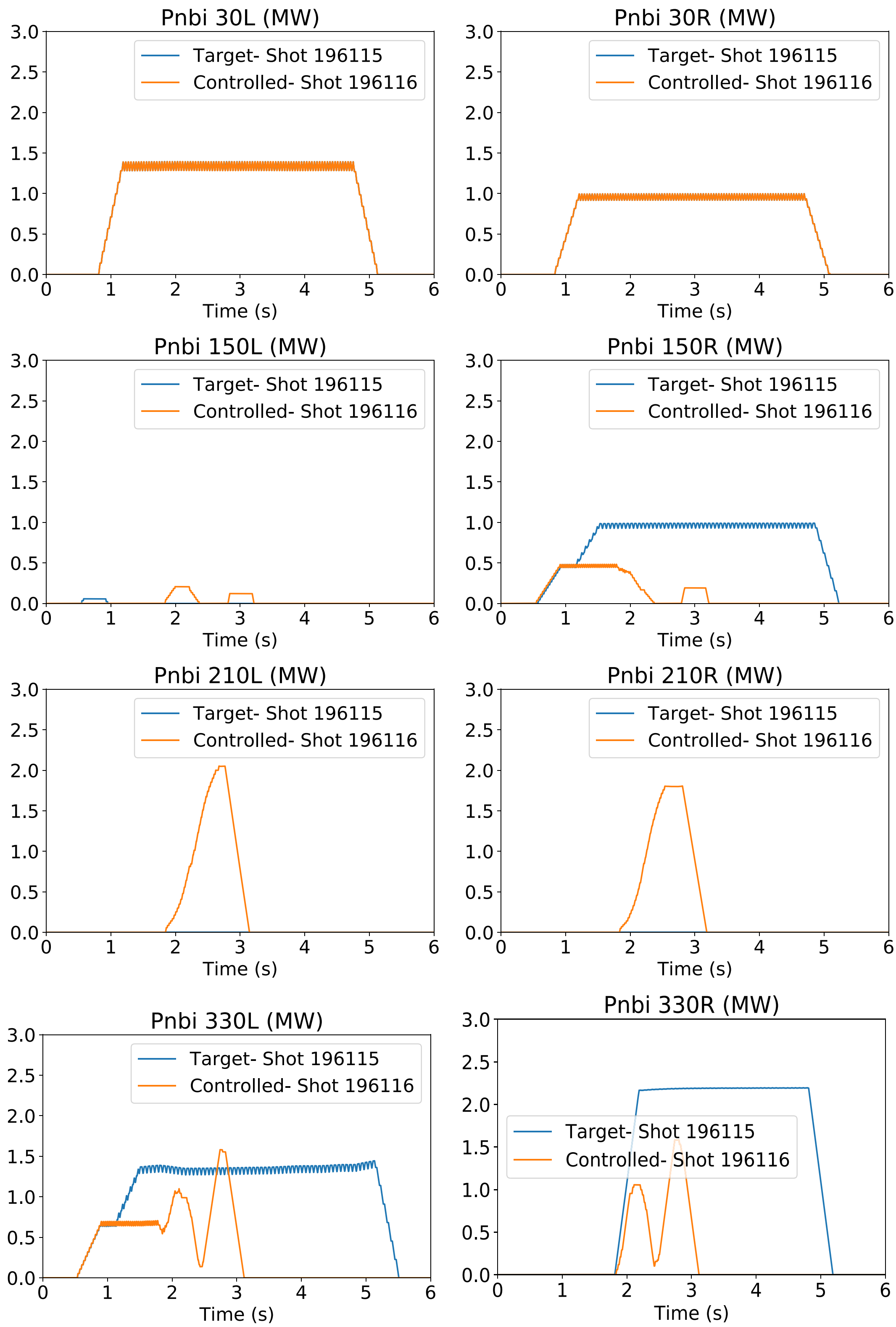

Figure 13. T_e controller neutral beam powers for shot 196116. The 30 L and 30 R beams are not included in feedback, so the controlled case perfectly matches the target case. More power is requested from the 210 and 330 beams, while less power is requested from 150 R.

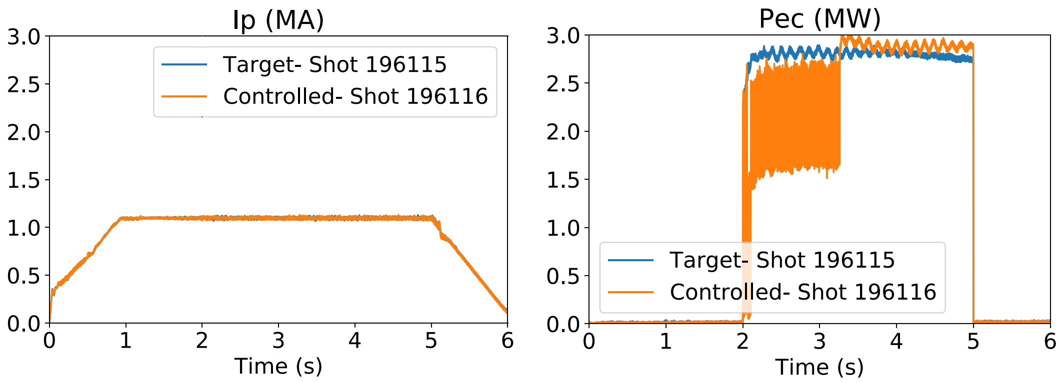

Figure 14. T_e controller current and ECH power for shot 196116. The plasma current for the controlled shot perfectly matched the plasma current for the target shot, while the ECH power for the controlled shot is similar but not an exact match to the target shot.

5. Conclusions and future work

In this work, a controller for the electron temperature profile was tested in experiment on DIII-D. A number of significant upgrades to the DIII-D PCS were necessary to enable this experiment. First, a set of neural network calculation capabilities were added in real time. This algorithm can currently run NubeamNet and MMMnet, but is set up to easily add any neural network of the PCAnet format. Next, an observer for the electron temperature profile was implemented in real time. This observer uses a combination of a predictive model (including contributions from NubeamNet and MMMnet) and diagnostic data from the Thomson scattering system to determine the state of the electron temperature profile in real time. This algorithm was tested in experiment, and proved to be capable of matching both the shape and the magnitude of the Thomson scattering data while producing a smooth, physically reasonable profile. The outputs of this observer were then used in a dedicated experiment to test the performance of the T_e profile controller. The results of this experiment demonstrated that the controller is capable of tracking a T_e target at spatial locations across the profile, and of compensating for disturbances and returning the temperature to the target state. Next steps for this controller include testing on a wider variety of target T_e profiles in a wider variety of plasma equilibria. A similar control scheme could also be implemented and tested on a longer pulse tokamak to demonstrate tracking of the target profile for a longer period of time.

This controller is intended for use in scenario development experiments to maintain the target plasma state; for this goal, it would be very desirable to be able to control multiple plasma profiles at the same time. For this purpose, it would be helpful to extend the LQI controller used in this experiment to include both the T_e profile and the q profile as targets. A simultaneous controller for both of these profiles has been developed and validated in simulation [27]. An experimental test of this simultaneous controller would require the same PCS framework as the T_e controller, including using the neural networks and the T_e observer. Now that these PCS tools are validated and available, they can be used for scenario development experiments employing the T_e profile controller, and they can also support other control development experiments such as testing the simultaneous T_e and q profile controller in real time.

Acknowledgments

The authors would like to thank Dr Ryan Chaban, Dr Zana Popovic, Dr Lauren Nuckols, and Professor Eva Kostadinova for allowing us to test the PCS implementation of the neural network models and the T_e observer algorithm during their experiments. This extra time was critical in making the dedicated experiment testing the T_e controller a success.

This material is based upon work supported by the U.S. Department of Energy, Office of Science, Office of Fusion Energy Sciences, using the DIII-D National Fusion Facility, a DOE Office of Science user facility, under Awards DE-FC02-04ER54698, DE-SC0010661, DE-SC0013977, and by the National Science Foundation Graduate Research Fellowship Program under Grant No. 1842163.

ORCID iD

S. Morosohk 0000-0002-3133-5095

References

[1] Mazon D. 2015 *Nucl. Instrum. Methods Phys. Res. B* **355** 101–6
[2] Walker M.L., De Vries P., Felici F. and Schuster E. 2020 Introduction to tokamak plasma control *Proc. 2020 American Control Conf.* (*Denver, CO*) pp 2901–18
[3] Felici F. *et al* 2017 Model-based design, simulation and testing of an electron temperature profile controller on ASDEX-Upgrade *EPS Plasma Physics Conf.* (*Belfast, Northern Ireland*) p 4
[4] Laborde L. *et al* 2004 *Plasma Phys. Control. Fusion* **47** 155
[5] Kim H.-S. *et al* 2018 *Fusion Eng. Des.* **135** 1
[6] Morosohk S.M., Wang Z., Paruchuri S.T., Rafiq T. and Schuster E. 2024 *Fusion Eng. Des.* **206** 114615
[7] Logan N., Grierson B.A., Haskey S.R., Smith S.P., Meneghini O. and Eldon D. 2018 *Fusion Sci. Technol.* **74** 125
[8] Groebner R. *et al* 2001 *Nucl. Fusion* **41** 1789
[9] Xing Z. *et al* 2021 *Fusion Eng. Des.* **163** 112163
[10] Shousha R., Seo J., Erickson K., Xing Z., Kim S., Abbate J. and Kolemen E. 2024 *Nucl. Fusion* **64** 026006
[11] Blanken T., Felici F., Rapson C., de Baar M. and Heemels W. 2018 *Fusion Eng. Des.* **126** 87
[12] Bosman T.O.S.J., van Berkel M. and de Baar M.R. 2021 *J. Phys. Commun.* **5** 115015
[13] Vincent B., Hudon N., Lefèvre L. and Dochain D. 2016 *IFAC-PapersOnLine* **49** 93–98
[14] Wang H., Barton J.E. and Schuster E. 2015 Poloidal flux profile reconstruction from pointwise measurements via extended Kalman filtering in the DIII-D tokamak *2015 IEEE Conf. on Control Applications (CCA)* (*Sydney, Australia*) pp 1309–14
[15] Felici F., Citrin J., Teplukhina A.A., Redondo J., Bourdelle C., Imbeaux F. and Sauter O. 2018 *Nucl. Fusion* **58** 096006
[16] Anderson B.D.O. and MOORE J.B. 1979 *Optimal Filtering* (Prentice-Hall)
[17] Morosohk S. and Schuster E. 2023 *Contrib. Plasma Phys.* **63** e202200153
[18] Boyer M. *et al* 2019 *Nucl. Fusion* **59** 056008
[19] Meneghini O. *et al* 2017 *Nucl. Fusion* **57** 086034
[20] Citrin J., Breton S., Felici F., Imbeaux F., Aniel T., Artaud J.F., Baiocchi B., Bourdelle C., Camenen Y. and Garcia J. 2015 *Nucl. Fusion* **55** 092001
[21] Morosohk S.M., Boyer M.D. and Schuster E. 2021 *Fusion Eng. Des.* **163** 112125
[22] Scoville J., Boyer M.D., Crowley B.J., Eidietis N.W., Pawley C.J. and Rauch J.M. 2019 *Fusion Eng. Des.* **146** 6
[23] Morosohk S.M., Pajares A., Rafiq T. and Schuster E. 2021 *Nucl. Fusion* **61** 106040
[24] Clement M., Logan N. and Boyer M. 2022 *Nucl. Fusion* **62** 026022
[25] Austin M. and Lohr J. 2003 *Rev. Sci. Instrum.* **74** 1457
[26] Wroblewski D. and Lao L. 1992 *Rev. Sci. Instrum.* **63** 5140
[27] Morosohk S., Wang Z., Paruchuri S.T., Rafiq T. and Schuster E. 2025 *Plasma Phys. Control. Fusion* **67** 015012